



The catalytic machinery of the FAD-dependent *AtBBE*-like protein 15 for alcohol oxidation: Y193 and Y479 form a catalytic base, Q438 and R292 an alkoxide binding site

Julia Messenlehner^{a,2}, Michael Hetman^{b,e,2}, Adrian Tripp^a, Silvia Wallner^a, Peter Macheroux^{a,c}, Karl Gruber^{b,c,d}, Bastian Daniel^{a,b,e,*}, 1, 1

^a Graz University of Technology, NAWI Graz, Institute of Biochemistry, Graz, Austria

^b University of Graz, NAWI Graz, Institute of Molecular Biosciences, Graz, Austria

^c BioTechMed-Graz, Graz, Austria

^d Field of Excellence BioHealth – University of Graz, Graz, Austria

^e Acib-Austrian Centre of Industrial Biotechnology, Krenngasse 37, Graz, Austria

ARTICLE INFO

Keywords:

Reaction mechanism
Flavoprotein
Structure-function relationship
Alcohol oxidase

ABSTRACT

Monolignol oxidoreductases are members of the berberine bridge enzyme-like (BBE-like) protein family (pfam 08031) that oxidize monolignols to the corresponding aldehydes. They are FAD-dependent enzymes that exhibit the para-cresolmethylhydroxylase-topology, also known as vanillyl oxidase-topology. Recently, we have reported the structural and biochemical characterization of two monolignol oxidoreductases from *Arabidopsis thaliana*, *AtBBE13* and *AtBBE15*. Now, we have conducted a comprehensive site directed mutagenesis study for *AtBBE15*, to expand our understanding of the catalytic mechanism of this enzyme class. Based on the kinetic properties of active site variants and molecular dynamics simulations, we propose a refined, structure-guided reaction mechanism for the family of monolignol oxidoreductases. Here, we propose that this reaction is facilitated stepwise by the deprotonation of the allylic alcohol and a subsequent hydride transfer from the C α -atom of the alkoxide to the flavin. We describe an excessive hydrogen bond network that enables the catalytic mechanism of the enzyme. Within this network Tyr479 and Tyr193 act concertedly as active catalytic bases to facilitate the proton abstraction. Lys436 is indirectly involved in the deprotonation as this residue determines the position of Tyr193 via a cation- π interaction. The enzyme forms a hydrophilic cavity to accommodate the alkoxide intermediate and to stabilize the transition state from the alkoxide to the aldehyde. By means of molecular dynamics simulations, we have identified two different and distinct binding modes for the substrate in the alcohol and alkoxide state. The alcohol interacts with Tyr193 and Tyr479 while Arg292, Gln438 and Tyr193 form an alkoxide binding site to accommodate this intermediate. The pH-dependency of the activity of the active site variants revealed that the integrity of the alkoxide binding site is also crucial for the fine tuning of the pK_a of Tyr193 and Tyr479. Sequence alignments showed that key residues for the mechanism are highly conserved, indicating that our proposed mechanism is not only relevant for *AtBBE15* but for the majority of BBE-like proteins.

1. Introduction

Flavoproteins are a diverse protein class utilizing the isoalloxazine ring in form of the flavin mononucleotide (FMN) or the flavin adenine dinucleotide (FAD) for catalysis [1,2]. A distinct set of recurrent features

of flavoproteins has been elaborated by Fraaije et al. [3]. Substrates for flavoproteins typically exhibit an activatable group, e.g. an alcohol is activated by deprotonation by a catalytic base, leading to the alkoxide, which transfers a hydride to the N5 atom of the isoalloxazine ring. Furthermore, it was also postulated that the distance of the oxidized

* Corresponding author. Institute of Molecular Biosciences, Humboldtstraße 50/3, 8010, Graz, Austria.

E-mail address: bastian.daniel@uni-graz.at (B. Daniel).

¹ current affiliation.

² Authors contributed equally.

<https://doi.org/10.1016/j.ab.2021.108766>

Received 26 October 2020; Received in revised form 11 January 2021; Accepted 12 January 2021

Available online 22 January 2021

0003-9861/© 2021 The Authors. Published by Elsevier Inc. This is an open access article under the CC BY license (<http://creativecommons.org/licenses/by/4.0/>).

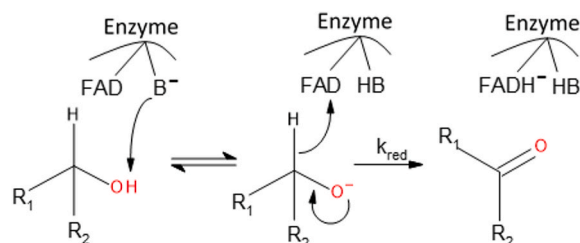
carbon, also referred to as site of oxidative attack, to the N5 and the angle to the N5-N10 axis are well defined and universal for the majority of flavoproteins independent of their structure [3]. The reaction scheme of an alcohol oxidation by a flavoprotein via hydride transfer is depicted in Scheme 1:

As indicated in Scheme 1, the substrate is activated prior to the hydride transfer and the alkoxide needs to be accommodated by the active site of the flavin dependent alcohol oxidoreductase [4]. Previously we have shown that AtBBE15 (At2g34790) and 13 (At1g30760) are FAD-dependent monolignol oxidoreductases and that there is a set of conserved residues in the active site [5,6]. The role of these residues in catalysis was now addressed by means of a site directed mutagenesis program using AtBBE15 as a model enzyme.

The BBE-like protein family was named after the berberine bridge enzyme (*EcBBE*) from *Eschscholzia californica* (*California poppy*) that catalyzes the conversion of (*S*)-reticuline to (*S*)-scoulerine [7,8]. BBE-like proteins occur in fungi, bacteria, archaea and plants. In the latter, they form a multigene family, the number of members varies from one in the moss *Physcomitrella patens* to 64 in western poplar (*Populus trichocarpa*) [9]. *Arabidopsis thaliana* has 27 genes coding for AtBBE-like proteins and recently we could identify two of them (AtBBE13 and 15) as monolignol oxidoreductases, oxidizing the monolignols to the corresponding aldehydes [5]. In the course of this study, we have solved the crystal structure of AtBBE15 and proposed a catalytic mechanism for the enzyme. Here, we present a site directed mutagenesis study to support and refine the postulated mechanism by the analysis of the kinetic properties of active site variants of AtBBE15 in conjunction with molecular dynamics simulations. The overall topology of AtBBE15 is shown in Fig. 1A. The enzyme can be divided into different modules; the N- and C-terminal FAD-binding modules are colored in purple and blue, respectively, and the BBE-motif is colored in red. The substrate-binding module is shown in green. At the interface of the FAD- and the substrate-binding module the isoalloxazine (depicted in orange) is located [6]. Near the N5 of the flavin, a set of polar residues is located forming the active site. They are depicted as stick models in Fig. 1B.

AtBBE15 forms a funnel shaped cavity consisting of a wide hydrophobic pocket and leading up to the active site close to the N5 of the cofactor that is predominantly formed by polar residues. As typical for this protein family, the FAD-cofactor is bivalently attached via a Cys115 and His179 to the enzyme. The residues in the active site form an extensive hydrogen bond network including two water molecules. The cavity was visualized and analyzed using the CASOX tool. In Fig. 2, an imprint of the cavity is shown with the surrounding residues and the hydrogen bond network that they form [10,11].

In the imprint of the cavity depicted in Fig. 2, hydrophobic areas of the cavity are shown in red while hydrophilic areas are colored in blue. The hydroxy group of Tyr117 has a 2.7 Å distance to the OE1 of Gln438. A water molecule is complexed by NE2 of Gln438 and ND2 of Asn411 with distances of 2.9 Å and 3.0 Å, respectively. Another water molecule is complexed by OD1 of Asn411 and NH1 of Arg292 with distances of 2.5



Scheme 1. Reductive half reaction of a flavin-dependent alcohol oxidation: The alcohol enters the active site, which features the FAD-cofactor (FAD) and a catalytic base B. The corresponding alkoxide is formed via deprotonation of the alcohol group. The corresponding aldehyde is formed via hydride transfer to the N5 position of the flavin.

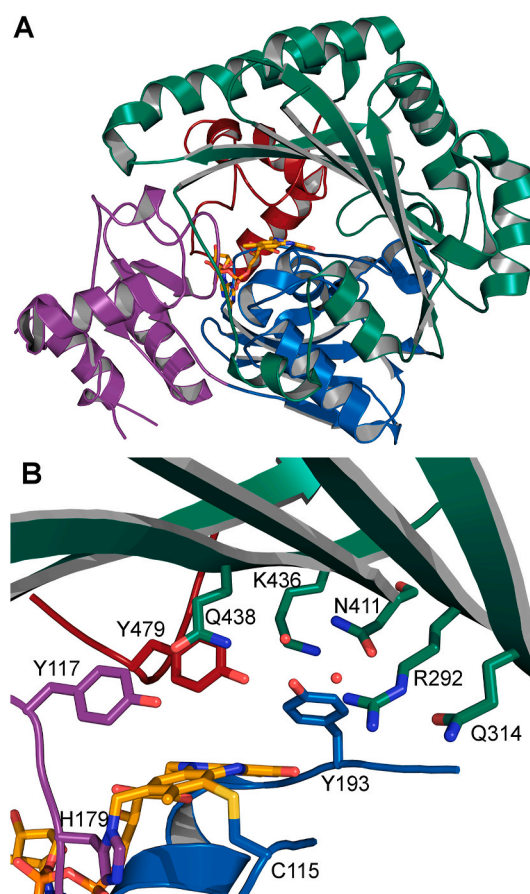


Fig. 1. A: Overall topology of AtBBE15; B: The residues that are forming the active site are depicted as stick models and colored according to the module they originate from.

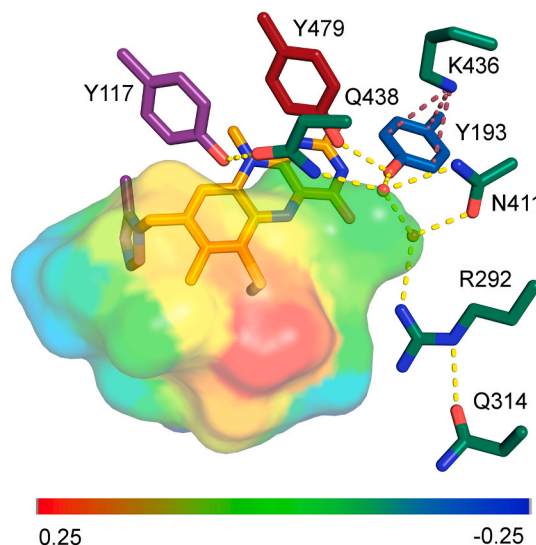


Fig. 2. Imprint of the substrate binding pocket of AtBBE15. Hydrophobic regions are colored in red, hydrophilic in blue. Polar interactions are shown in yellow, cation- π interactions in purple.

and 3.0 Å, respectively. A 2.9 Å hydrogen bond is between NE of Arg292 and OE1 of Gln314. These interactions represent a hydrogen bond network connecting Tyr117 to Gln438 over a water molecule to Asn411 over a water molecule to Arg292 that interacts with Gln314. Previously,

we have postulated a productive binding mode of coniferyl alcohol in the active site [5]. Taking into account this conformation, Tyr117 and Gln314 are to be anticipated as second shell residues that do not participate directly in the reaction but are important interaction partners to Gln438 and Arg292, respectively. Additionally, the hydroxyl groups of Tyr193 and Tyr479 are in close proximity to each other forming a 2.5 Å hydrogen bond. The aromatic ring of Tyr193 is engaged in a cation- π interaction with the side chain amino group of Lys436. In addition, a 2.6 Å hydrogen bond between the hydroxy group of Tyr193 to the water molecule complexed by Gln438 and Asn411 is formed.

2. Experimental and procedures

2.1. Mutagenesis, protein production and purification

Mutagenesis was conducted as described in Daniel et al., protein production and purification was done as reported before [5]. The variants were analyzed via SDS-Page, no difference to the wild-type enzyme were observed, a respective gel is depicted in the supplemental file as Figure S1. The synthetic gene sequence was published before, the respective primers are listed in Table 1 [12].

Screening was performed according to Weis et al. in 96 well plates [13]. After 72 h of induction the cells were separated from the supernatant by centrifugation, the supernatant was employed for immunodetection as described before for the wild type enzyme. Additionally, an activity assay in a microtiter plate was conducted using 50 μ L supernatant and 30 μ L of a saturated DCPIP solution containing 1.33 mM coniferyl alcohol with a *Komagataella phaffii* (formerly known as *P. pastoris*) strain expressing wild type AtBBE15 as positive control. Enzyme activity was indicated by the decolorization of the blue dye, which is easily detectable by visual inspection. Both methods were found to be suitable for the identification of expression strains for all variants except for the Tyr193Phe variant. For this variant, transformants could be identified by immunodetection but no enzyme activity could be observed in the supernatant.

2.2. Spectral properties

To determine the UV/Vis-absorption spectra of the native flavoproteins, they were diluted to an absorbance of 0.1 at 450 nm in 50 mM Tris and 150 mM NaCl, pH 8 and the spectra were recorded from 300 to 800 nm. 100 μ L 10% SDS solution was added and the enzyme solution was heated for 30 min at 95 °C. Afterwards the spectra were recorded again employing a Specord 205 spectrometer (Analytik Jena AG, Jena, Germany).

2.3. Rapid reaction kinetics using stopped flow

Kinetic measurements were conducted as previously reported for the wild type enzyme [5]. Prior to kinetic measurements the activity of the variants was verified employing coniferyl alcohol as a substrate. Spectra of the oxidized and reduced variants were recorded employing a Specord 205 spectrometer (Analytik Jena AG, Jena, Germany). The respective variants were diluted depending on their spectral properties to give an absorbance of 0.2 at 450 nm in 50 mM potassium phosphate buffer pH

7.0. The spectra of the substrate reduced species were recorded after the addition of coniferyl alcohol to a final concentration of 40 μ M. The respective enzyme solutions were used for the stopped-flow experiments.

2.4. Steady state kinetics

Assays were performed in buffers with 100 mM citrate and 150 mM NaCl (pH 3–6), 100 mM potassium phosphate and 150 mM NaCl (pH 6–7.75) or 100 mM Tris and 150 mM NaCl (pH 8–9), a final concentration of 500 μ M cinnamyl alcohol in doubly distilled H₂O as substrate and a final concentration of 120 μ M DCPIP in H₂O as electron acceptor. Buffer, substrate and DCPIP were incubated at 25 °C for 2 min in a cuvette. 20 μ L of the respective AtBBE15 variant was added to a final volume of 1 mL and thoroughly mixed. The decreasing absorption was recorded for 160 s. All samples were measured in triplicates at 25 °C. The decreasing absorption over time was transformed to decreasing concentration of DCPIP over time by its extinction coefficient at the respective pH values which was determined with a DCPIP stock solution and were in good agreement with previously published data. All ingredients except the enzyme were used in the same concentration as reference.

2.5. Protein-ligand docking

For docking of coniferyl alcohol in AtBBE15 AutoDock Vina was used [14]. The docking box was limited to the active site of the protein and centered around the N5-atom of FAD. 25 docking runs were calculated and docking modes with a maximum RMSD of 5 Å were clustered together. The chemically most meaningful docking mode was chosen as a starting point for the molecular dynamic simulations.

2.6. Molecular dynamics (MD) simulation

The MD simulations were carried out using Desmond [15]. The chosen docking mode was selected as a starting point for the simulation of AtBBE15 with bound coniferyl alcohol. An orthorhombic simulation box was placed around the protein and the water box was calculated. After the equilibration, a 400 ns long NPT – MD simulation was calculated. The Martyna-Tobias-Klein barometer and Nose-Hoover chain thermostat functions were used. For the MD simulation of AtBBE15 with bound coniferyl alkoxide the protonation states of the initial docking mode were changed. Coniferyl alcohol was deprotonated and Tyr193 was protonated. To avoid unwanted effects during equilibration, which lead to a significantly altered orientation of active site residues (compared to the crystal structure) the charged Lys436 was mutated to the non-charged methionine (for the simulation of AtBBE15 with bound coniferyl alkoxide). For the MD simulation with the alcohol and the respective alkoxide the same parameters were used. The resulting trajectories were analyzed using Desmond and VMD3.

2.7. Sequence alignments

Sequences were retrieved from the Phytozome v12.1 [16]. For monocotyledons in total 171 sequences from all genomes currently

Table 1
Primer for site directed mutagenesis 5'-3'.

Mutation	Forward primer	Reverse primer
N411V	CACCGTTAACGATATGGGTCCCTACGGAGGAATGATG	CATCAITCCTCCGTAAGGGACCCATATCGTTAACGGTG
Y117F	GCGGTGGTCACGACTTCGAAGGGCTCTCG	CGAGAGCCCTTCGAAGTCGTGACCACCGC
Q438V	ACATTGTTCAAGATTGTGTGGCTAAGCACGTGGC	GCCACGTGCTTAGCCACACAATCTGAACAATGT
K436L	GGMCGGGACATTGTTCTGATTCAGTGGCTAAGC	GCTTAGCCACTGAATCAGGAACAATGTCCCGTTCC
Y193F	CTTAGTCGGTGGAGCGTTTCGGTTCATGATGAGG	CCTCATATGGAACCGAA CGCTCCACCGACTAAG
R292 M	GACGATGATCTCTTCATTATGGTCATTATTCACCGGCCAG	CTGGCCGGTGAATAATGACCATAATGMGAGATCATCGTC
Y479F	GACAGGCCTATGTGAATT TCAGGGATCTTGATTTGGGG	CCCCAAATCAAGATCCCTGAAATTCACATTAGGCCTGTG

available (*Marchantia polymorpha*, *Physcomitrella patens*, *Selaginella moellendorffii*, *Ananas comosus*, *Amborella trichopoda*, *Musa acuminata*, *Spirodela polyrhiza*, *Zostera marina*, *Brachypodium distachyon*, *Brachypodium stacei*, *Oryza sativa*, *Oropetium thomaeum*, *Panicum hallii*, *Panicum virgatum*, *Setaria italica*, *Setaria viridis*, *Sorghum bicolor*, *Zea mays* PH207 and *Zea mays* PH207; Date September 2020) were retrieved, aligned using Clustal omega and edited by hand using Jalview [17,18]. For dicotyledons 272 sequences from selected representative species (*Aquilegia coerulea*, *Amaranthus hypochondriacus*, *Eucalyptus grandis*, *Populus trichocarpa*, *Arabidopsis thaliana*, *Gossypium raimondii*, *Solanum tuberosum*, *Medicago truncatula* and *Glycine max*, date September 2020) were retrieved and processed as described above. The respective alignments are deposited as Supplemental File S1 and S2.

3. Results and discussion

3.1. Spectral properties of the AtBBE15 variants

Based on the structure of AtBBE15 and our docking experiments (see below), we have generated the following active site variants: Tyr117Phe, Tyr193Phe, Arg292Met, Asn411Val, Lys436Leu, Gln438Val and Tyr479Phe. These variants were produced and purified as described before [5]. For an initial characterization, the UV/VIS absorption spectra of the purified proteins were recorded (see Fig. 3, panel A; wild type, Tyr193Phe, Arg292Met Gln438Val and Tyr479Phe and B; wild type, Tyr117Phe, Asn411Val and Lys436Leu). The UV/VIS absorption spectra of the respective denatured variants are depicted in panels C and D.

The spectral properties of AtBBE15 indicate the presence of a flavin cofactor, as typical for this protein family. The flavin spectrum of the wild-type enzyme is characterized by two peaks at 375 nm and 450 nm, both of them are assigned to a $\pi \rightarrow \pi^*$ transition [19]. In the free flavin spectrum a relative intensity A_{375}/A_{450} of 0.82 is observed, while for the flavin bound to AtBBE15 A_{375}/A_{450} is 1.33. Instead of the typical flavin double peak the enzyme exhibits a peak at 450 nm, a shoulder at 370 nm and strong absorption at 300 nm that is caused by a currently

not yet identified species. The perturbation of the spectrum can be caused by different electronic states other than the fully oxidized FAD cofactor. This has been reported for related enzymes from the VAO family, which were found to be expressed with a stable anionic semiquinone species of the flavin cofactor [20]. Also, the formation of adducts was found to perturb the flavin spectrum. Similar spectral properties were observed for the closely related BBE-like proteins PpBBE1 from *Physcomitrella patens* and Phl p 4 from timothy grass [21, 22]. For both enzymes a significant unresolved electron density was found in the active site (pdb codes 6EO4 and 3TSH, respectively). Nevertheless, the 450 nm peak of AtBBE15 was diminished upon photoreduction or by titration with coniferyl alcohol and upon reoxidation the absorption returned to its original level. Therefore, the absorption at 450 nm is assigned to fully functional enzyme and can be exploited for the determination of kinetic parameters.

It should be noted that the spectral properties of the Tyr193Phe and Tyr479Phe variants drastically differ from the wild type enzyme. The spectra are dominated by a peak at 390 nm (compare Fig. 3 panel A). While for the Tyr479Phe variant a residual absorption at 450 nm can be observed, that is diminished upon reduction by substrate, this is not the case for the Tyr193Phe variant. The alteration of the active site might make these two variants more susceptible to the not yet identified modification of the flavin cofactor, hence the spectrum of the Tyr193Phe variant is anticipated to resemble that of the flavin-adduct species that is catalytically inactive. All other spectra can be interpreted as two overlapping spectra from the fully oxidized catalytically functional FAD and the modified FAD-cofactor. The exact nature of this modification is to be identified in future work. For the variants Asn411Val, Gln438Val, Arg292Met, Lys436Leu and Tyr117Phe a peak at 450 nm, a shoulder at 350 and strong absorption at 320 nm was observed. All of them were found to be substrate reducible. Upon denaturation BBE-like proteins were found to have a characteristic absorption spectrum featuring a dominant peak at 440 nm that is assigned to the 6-cysteinyl-FAD, the spectra are depicted in Fig. 3 panel C and D [23]. For the Gln438Val, Lys436Leu, Tyr117Phe, Tyr479Phe variants the same ratio of A_{320}/A_{440} is observed as for the wild type. The Arg292Met and

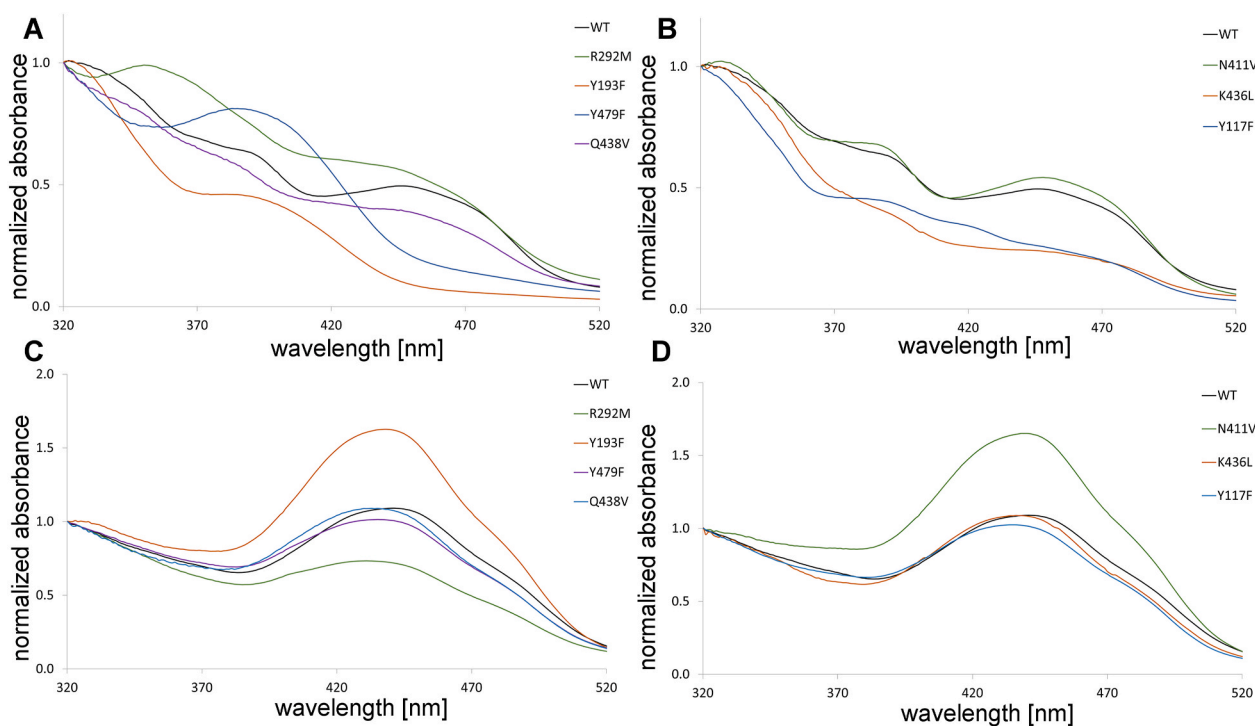


Fig. 3. Spectral properties of the AtBBE15 variants and wild type. Panel A and B: UV/VIS absorption spectra of the native enzymes, panel C and D: Spectra of the denatured enzymes. All spectra were normalized at 320 nm.

Tyr193Phe variants show an increased absorption at 440 nm while the Asn411Val variant shows a decrease, respectively.

3.2. Rapid reaction kinetics using stopped flow

The reductive half reaction was determined for all variants employing *p*-coumaryl alcohol and cinnamyl alcohol as substrates. The observed rates are summarized in Fig. 4 (panel A: *p*-coumaryl alcohol, panel B: cinnamyl alcohol). As the reaction follows pseudo first order kinetics, the observed rates were calculated by a mono-exponential fit with exception of the Tyr479Phe variant for which a bi-exponential fit was used.

In Fig. 4, the observed rates determined by pre-steady-state kinetics employing cinnamyl alcohol and *p*-coumaryl alcohol as reducing agents for all active site variants with exception of AtBBE15 Tyr193Phe are shown. The reductive rates k_{red} and the dissociation constants K_d were calculated from the observed rates determined with *p*-coumaryl alcohol. Due to solubility limitation the saturation phase cannot be reached with cinnamyl. The kinetic data is summarized in Table 2. The limiting rate (k_{red}) and the observed rate (k_{obs}) determined at a concentration of 500 μ M cinnamyl alcohol with wild type enzyme, were set to 100% to compare the impact of the active site variations.

The kinetic data listed in Table 2 reveal that with all variants analogous effects on k_{red} or k_{obs} were determined for both substrates. Severe effects have been observed for the variants Gln438Val, Tyr117Phe and Arg292Met with a residual k_{red} of 6%, 6% and 9%, respectively. Also,

the substrate binding is affected leading to an increased K_d of $2890 \pm 87 \mu$ M, $1408 \pm 202 \mu$ M and $1408 \pm 202 \mu$ M if compared to the K_d of the wild type enzyme of $665 \pm 85 \mu$ M. Moderate effects have been observed for the variants Asn411Val and Lys436Val with residual k_{red} amounting to 43% and 22% compared to wild-type protein, respectively, and increased K_d of $1505 \pm 70 \mu$ M and $2024 \pm 61 \mu$ M, respectively. Although for all other variants a monoexponential decay of the absorption at 450 nm was observed in the stopped flow experiments, for the Tyr479Phe variant a biexponential decay with a ratio of phase 1 (p1) to phase 2 (p2) of 2:1 was found. Interestingly, p1 was found to exhibit 463% of the wild type k_{obs} , k_{red} , however, could not be determined due to dead time limitations. With 50 μ M *p*-coumaryl alcohol, k_{obs} of the Tyr479Phe variant was found to be increased to 336%. For p2, k_{obs} was found to be decreased to 19%, k_{red} was determined to be 9% while K_d was increased to $2097 \pm 95 \mu$ M. In a study on the FAD-dependent vanillyl alcohol oxidase (VAO) two tyrosine residues are proposed to be responsible for the deprotonation of the phenolic substrate prior to oxidation [24]. Analogous to the Tyr479Phe variant, different rates were determined for a slow and a fast phase regarding the hydride transfer as observed in pre-steady-state kinetics with the respective VAO variants. Ewing et al. assigned the fast phase to the reaction of the deprotonated, *i.e.* activated substrate, while the slow rate was assigned to the reaction of the enzyme with the protonated substrate, in other words, the enzyme is much slower because the catalytic base is not in the right protonation state for substrate activation. For AtBBE15 we suggest a model analogous to Ewing's findings for the reductive half reaction that is depicted in Scheme 2 with E representing the enzyme and S the substrate.

Tyr193 and Tyr479 concertedly act as catalytic base and are in an equilibrium between the inactive fully protonated and the half-deprotonated form E_{ox}^- . Both states can bind the substrate leading to a productive enzyme substrate complex [$E_{ox}^- + SH$] or the less-productive enzyme substrate complex [$E_{ox}H + SH$]. In the productive enzyme substrate complex the substrate can be activated and the subsequent hydride transfer is determined by k_{obs1} . Additional steps are necessary from the less-productive enzyme substrate complex to the product formation leading to second rate k_{obs2} , which is slower than k_{obs1} .

To evaluate the impact on catalysis caused by the amino acid variations that were introduced in the active site of AtBBE15, Equations (1) and (2) were used [25,26], where $\Delta\Delta G_T^\ddagger$ signifies the change in the stabilization of the transition state energy while $\Delta\Delta G^\ddagger$ reflects the activation free energy of the reaction. Using the values in Table 2, we calculated $\Delta\Delta G^\ddagger$ and $\Delta\Delta G_T^\ddagger$ for the AtBBE15 variants (Table 3).

$$\Delta\Delta G_T^\ddagger = -RT \ln \left(\frac{(k_{red}/K_d)^{variant}}{(k_{red}/K_d)^{wt}} \right) \quad (1)$$

$$\Delta\Delta G^\ddagger = -RT \ln \left(\frac{k_{red}^{variant}}{k_{red}^{wt}} \right) \quad (2)$$

The calculated values in Table 3 indicate that each residue in this extensive network has limited contribution of 5–11 kJ/mol to the transition state stabilization. In general, a more pronounced effect is observed for $\Delta\Delta G_T^\ddagger$ than for $\Delta\Delta G^\ddagger$, indicating that the variations affect the stabilization of the transition state more than the substrate binding. The stabilization of the transition state for the variants AtBBE15 Gln438Val, Arg292Met and Tyr117Phe varied by 11, 9, and 9 kJ/mol respectively. A minor change of $\Delta\Delta G_T^\ddagger$ for the Lys436Leu and Asn411Val variants with 6 and 5 kJ/mol was calculated.

3.3. Steady-state kinetics

In addition to pre-steady-state kinetics, we investigated steady state kinetics in the pH range from 5 to 9 employing cinnamyl alcohol and DCPIP as the terminal electron acceptor. The relative pH-dependent velocities of the respective variants are depicted in Fig. 5. The

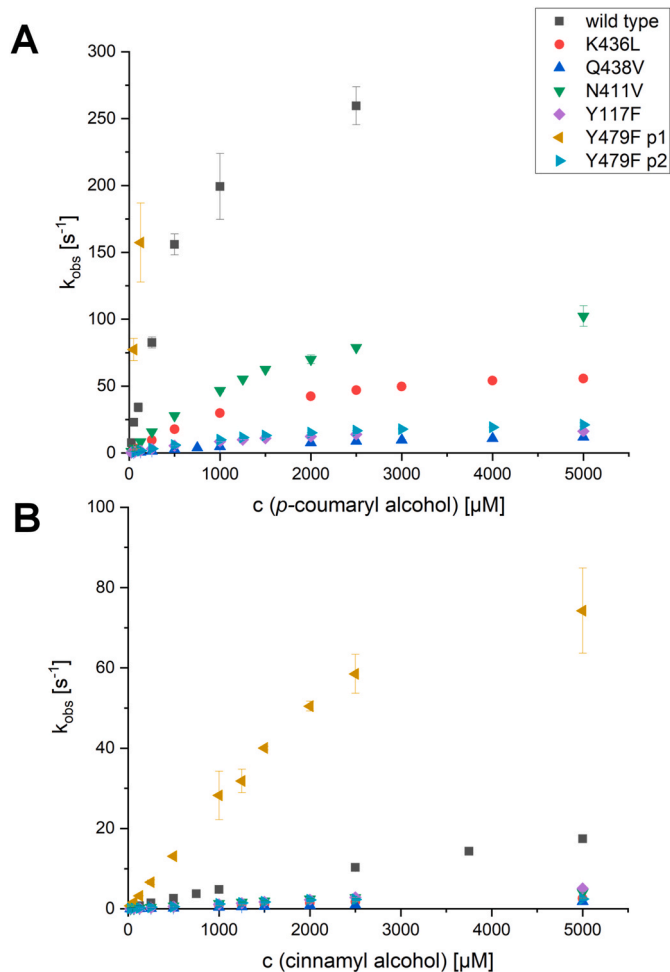
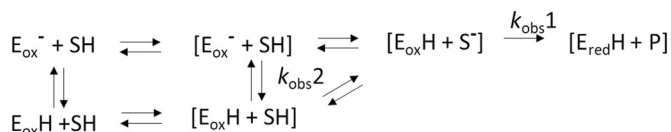


Fig. 4. Rates observed for the reductive half-reaction of AtBBE15 variants determined with cinnamyl alcohol (panel A) and *p*-coumaryl alcohol (panel B) by stopped-flow kinetics.

Table 2Kinetic parameters and dissociation constants of the AtBBE15 variants. * k_{obs} determined at 50 μM , ** not determined due to dead time limitation, *** taken from [5].

variant	<i>p</i> -coumaryl alcohol		cinnamyl alcohol		
	k_{red} [s^{-1}]	k_{red} [%]	K_d [μM]	k_{obs} [s^{-1}]	k_{obs} [%]
wild type***	332 ± 17	100	665 ± 85	2.6 ± 0.1	100
K436L	74 ± 1	22	1505 ± 70	0.42 ± 0.01	16
Q438V	19 ± 0.3	6	2890 ± 87	0.20 ± 0.02	8
N411V	143 ± 2	43	2024 ± 61	0.70 ± 0.01	26
Y117F	21 ± 2	6	1408 ± 202	0.56 ± 0.01	21
Y479F p1	nd**	336*	nd**	12 ± 0.90	462
Y479F p2	31 ± 1	9	2097 ± 95	0.49 ± 0.10	19
R292 M	29 ± 1	9	1873 ± 106	0.15 ± 0.03	12

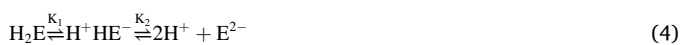


Scheme 2. Proposed model for the reductive half-reaction of AtBBE15: The enzyme E harbors a FAD-cofactor, therefore it can adopt an oxidized or a reduced state (E_{ox} or E_{red}), additionally the catalytic base can be protonated or deprotonated (EH , E^-). Depending on the protonation state a productive ($[E_{\text{ox}} + \text{SH}]$) or a less-productive enzyme-substrate complex ($[E_{\text{ox}}\text{H} + \text{SH}]$) can be formed giving rise to two different rates $k_{\text{obs}}1$ and $k_{\text{obs}}2$.

obtained velocities were fitted using Equation (3) with v = relative velocity and f = scaling factor to determine the pH optimum and the $\text{p}K_a$ values (Table 4).

$$v = f^* \frac{10^{pH - \text{p}K_a}}{1 + 10^{pH - \text{p}K_a} + 10^{2pH - \text{p}K_a - \text{p}K_a2}} \quad (3)$$

The titration curves were found to be bell shaped indicating that the active site of the enzyme (E in equation 4) behaves as a doubly ionizing system following Equation 4.



For the wild-type enzyme a pH optimum of 7.2 ± 0.2 with a $\text{p}K_{a1}$ and a $\text{p}K_{a2}$ of 6.2 ± 0.1 and 8.3 ± 0.2 was determined, which is in good agreement with previously published data employing the Leu182Val variant [27]. Previously, we have postulated that Tyr193, Tyr479 and Lys436 act concertedly to form a catalytic base [5]. The first ionization event characterized by the $\text{p}K_{a1}$, we assign to the deprotonation of either Tyr193 or Tyr479. The close proximity of their hydroxyl groups of 2.5 Å indicates a strong hydrogen bond, that meets the criteria described in literature for low barrier hydrogen bonds, i.e. a similar $\text{p}K_a$ value and a distance of <2.5 Å [28]. In the catalytically active state of the enzyme, we postulate that Tyr193 and Tyr479 share a proton and therefore act as catalytic base to activate a given substrate via proton abstraction. The second ionization event characterized by $\text{p}K_{a2}$, we assign to the deprotonation of the N3 position of the isoalloxazine ring with a reported $\text{p}K_a$ value of ≈ 10 [29]. We presume that a negative charge at the N3-position of the isoalloxazine ring impedes hydride transfer to the N5-position and thereby deactivates the enzyme at higher pH values. The strongest effect on the $\text{p}K_{a1}$ with a shift of more than two units was determined for the

Table 3

Changes in activation energy and the free energy change of AtBBE15 variants.

	$\Delta\Delta G_T^\ddagger$ [kJ mol^{-1}]	$\Delta\Delta G^\ddagger$ [kJ mol^{-1}]
K436L	6	4
Q438V	11	7
N411V	5	2
Y117F	9	7
R292 M	9	6

Gln438Val variant. The Gln438 interacts with Tyr117 and determines thereby the position of the terminal amide group. The NE of Gln438 interacts with Tyr193 via a water molecule that is complexed by Asn411 and Gln438 (see Fig. 2), also an electrostatic interaction with Tyr479 over a distance of 3.1 Å putatively explains the strong influence of Gln438 on the acidity of Tyr479 and Tyr193. The effect on $\text{p}K_{a2}$ with a shift of 0.5 units in the Gln438Val variant is less pronounced as no direct interaction to the N3 of the isoalloxazine ring is given. In the Arg292Met variant the $\text{p}K_{a1}$, pH_{opt} and $\text{p}K_{a2}$ are each shifted approximately 1 unit. The positively charged guanidino group contributes also to the overall electrostatic properties of the active site, the loss of this charge affects Tyr193, Tyr479 and N3 equally. There is the general tendency that the variations lead to an increase of $\text{p}K_{a1}$, the pH_{opt} and $\text{p}K_{a2}$ with exception of the Asn411Val variant. From this, we conclude that one purpose of the excessive hydrogen bond network is to keep the active site in an ionization state enabling the activation of the substrate via proton abstraction.

AtBBE15 was found to be part of the *Arabidopsis* cell wall proteome, the apoplastic pH can range from 5 to 7, i.e. it matches the pH-optimum of the enzyme [30]. With the exception of the Asn411Val variant, all variants showed an increased pH optimum, i.e. each variation shifts the pH optimum out of the physiological area and conversely each of the highly conserved active site residues contribute to the adaption of the enzyme to its environment *in planta*.

3.4. Docking

To assess the binding of monolignols to AtBBE15, coniferyl alcohol was chosen as an example of a monolignol and docked to the active site. To observe the binding of the substrate in a productive active site composition, Tyr193, which could serve as the catalytic base needed for the initial proton abstraction, was deprotonated. Furthermore, the docking served as a starting point for the molecular dynamics simulation.

The docking mode displayed in Fig. 6 was chosen as a starting point for the following MD simulation.

3.5. Molecular dynamics simulations

For analysis, the time period with a productive docking mode of coniferyl alcohol in the active site of AtBBE15 was further investigated to determine how the enzyme interacts with the coniferyl alcohol or the alkoxide intermediate and which interactions within the active site residues are important to catalyze the reaction. Therefore, the first 100 ns of the simulation were analyzed and a snapshot structure was saved every 10 ps. The trajectories were analyzed regarding possible interactions of active site residues with the ligand and to other active site residues. For a hydrogen bond a distance cut-off parameter of 3.2 Å and an angle criterion of $90^\circ \leq \alpha \leq 180^\circ$ (for the angle D-H-A) were used. In Table 5, the percentages of snapshot structures (during the 100 ns simulation) in which the criteria for a certain interaction is fulfilled are listed [31,32].

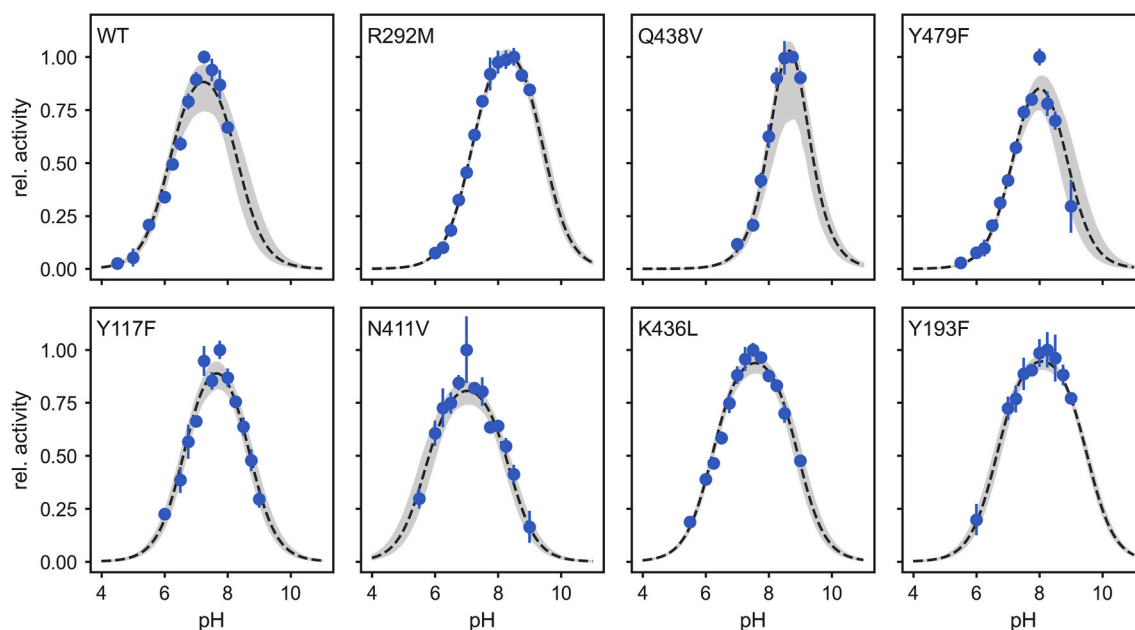


Fig. 5. Fit to the pH-dependent activity data of wild-type AtBBE15 and its variants. Activity data are shown as blue circles with the error bar representing the standard deviation from three replicates. Non-linear least-squares was performed using the function 'curvefit' from the scipy-module in python. The best fit is shown as a dashed line, the grey area represents the 95% prediction interval obtained by a bootstrapping procedure. (For interpretation of the references to color in this figure legend, the reader is referred to the Web version of this article.)

Table 4

pH optima, pK_{a1} and pK_{a2} derived from the pH dependency of the reaction velocity and Equation (3).

	pK_{a1}	pH_{opt}	pK_{a2}
WT	6.2 ± 0.1	7.2 ± 0.2	8.3 ± 0.2
R292 M	7.2 ± 0.0	8.3 ± 0.1	9.4 ± 0.1
Q438V	8.4 ± 0.1	8.7 ± 0.3	8.9 ± 0.2
Y479F	7.2 ± 0.1	8.0 ± 0.2	8.8 ± 0.2
Y117F	6.6 ± 0.1	7.7 ± 0.1	8.7 ± 0.1
N411V	5.7 ± 0.1	7.0 ± 0.2	8.4 ± 0.1
K436L	6.2 ± 0.1	7.6 ± 0.1	8.9 ± 0.1
Y193F	6.7 ± 0.1	8.1 ± 0.1	9.5 ± 0.1

Table 5

Percentage of time points in which an interaction is possible between the active site residues and the allylic alcohol of conferyl alcohol (Ligand O1).

Interaction	AtBBE15 with conferyl alcohol	AtBBE15 with conferyl alkoxide
	% of time points with interaction	% of time points with interaction
Arg292-Asn411	99	85
Arg292-Gln314	99	97
Arg292-Ligand O1	1	61
Gln438-Tyr117	96	45
Gln438-Ligand O1	24	39
Tyr193-Ligand O1	85	79
Tyr479-Ligand O1	81	23
Tyr193-Tyr479	29	98

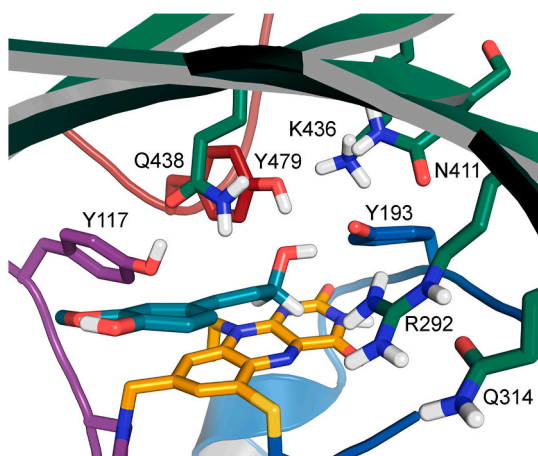


Fig. 6. Selected docking mode of conferyl alcohol bound to AtBBE15. All active site residues involved in the binding are shown. The hydroxyl group of conferyl alcohol mainly interacts with Tyr193 and Tyr479. The hydroxy group of Tyr193 was deprotonated and is therefore negatively charged.

3.6. Interaction of active site residues with the ligand

In the trajectory of AtBBE15 with bound conferyl alcohol two main interactions of the ligand with active site residues were detected. An interaction of the allylic alcohol substrate with Tyr193 and Tyr479 is possible in 85% and in 81% of the observed snapshot, respectively. Also, an interaction of Gln438 with the hydroxyl group of the ligand was observed in 24% of the snapshots. In the trajectory of AtBBE15 with bound conferyl alkoxide a different set of interactions was observed. The interaction between Tyr479 and the hydroxy group of the ligand was only given in 23% of the snapshots. The percentage of possible interaction of Tyr193 with the ligand is not significantly reduced and amounts to 79%. The interaction between ligand and Gln438 is possible in 39% of the snapshots and the interaction of Arg292 with the ligand is possible in 61% of the snapshots. The possibility of this interaction was only possible in 1% of the snapshots for the trajectory with bound conferyl alcohol. According to the docking results two different sets of interactions exist for conferyl alcohol and the respective alkoxide.

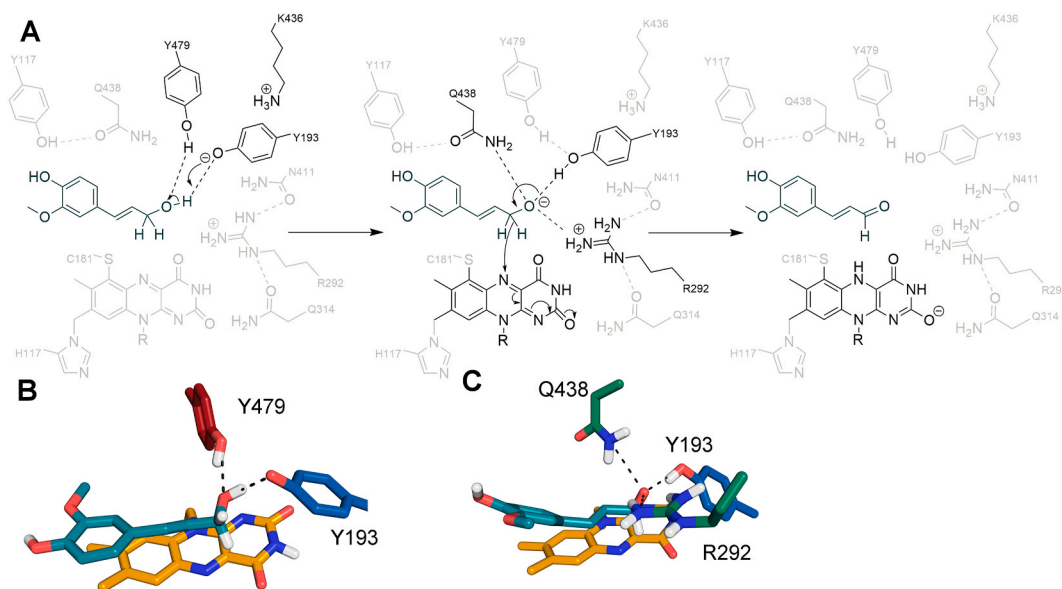


Fig. 7. Proposed catalytic mechanism of the alcohol oxidation of AtBBE15: The coniferyl alcohol interacts with Tyr193 and Tyr479 and is activated via proton abstraction (panel B). The respective alkoxide is complexed by Gln438, Arg292 and Tyr193, from this complex the hydride transfer to the FAD occurs (panel C).

Coniferyl alcohol predominantly interacts with Tyr193 and Tyr479, while the interaction of the enzyme with the corresponding alkoxide is realized via Gln438, Arg292 and Tyr193 (see Fig. 7).

3.7. Interactions among active site residues

An interaction between Arg292 and Asn411 and between Arg292 and Gln314 is possible in the majority of snapshots in both trajectories. Also, the possibility of an interaction between Tyr117 and Gln438 can be observed in both trajectories. We suggest that this interaction of residues plays a role in the positioning of the residues that interact directly with the ligand. The interaction of Arg292 and Gln438 with the ligand facilitates a positioning of the site of oxidative attack towards the N5 of the FAD that makes the hydride transfer possible.

3.8. Hydride transfer

For the possibility of a hydride transfer – necessary for the formation of coniferyl aldehyde - values observed in the literature were applied as criteria (Distance C-N5 < 3.8 Å, Angle N10-N5-CH: > 96 and < 162) [3]. In approximately 26% of time points observed, the hydride transfer would be possible, *i. e.* a productive binding mode was examined in our MD-simulations.

3.9. Proposed mechanism

We have postulated a step-wise mechanism for AtBBE15 and 13 based on kinetic data generated with wild-type enzymes. Alcohol oxidations by FAD-dependent enzymes typically involve the hydride transfer from an alkoxide intermediate, nevertheless a concerted mechanism cannot completely be ruled out [4,33,34]. In this study, we extended this work by generating active site variants and conducting a kinetic evaluation of the effects caused by the amino acid replacements. In conjunction with the docking and the MD-simulations, we propose a refined catalytic mechanism as depicted in Fig. 7 [5].

Initially the coniferyl alcohol enters the active site and the aromatic moiety is located in a hydrophobic cavity (see Fig. 2) while the alcohol moiety interacts with Tyr193 and Tyr479. The O-O distance of the tyrosine residues in the crystal structure of AtBBE15 (pdb code 4UD8) was found to be 2.4 Å and 2.5 Å, respectively, for chain A and B, bonds with these characteristics have been described as low barrier hydrogen

bonds [28]. We propose that Tyr193 and Tyr479 share a proton and therefore have a negative charge distributed over both residues to facilitate the substrate activation via proton abstraction. Lys436 contributes to the tuning of the pKa through formation of a cation- π interaction. Once the corresponding alkoxide is formed, a new hydrogen bond network around the intermediate is established as shown by our MD-simulations. The alkoxide interacts directly with Gln438, Arg292 and Tyr193. Gln438 forms a hydrogen bond to Tyr117 that defines the position of Gln438. The variation Tyr117Phe was found to have the same effect on k_{red} and K_d as in the Gln438Val variant emphasizing the importance of this highly conserved residue. Likewise, Arg292 interacts with Asn411 and Gln314 defining the position of this highly conserved residue. Concidentally they form a hydrophilic pocket around the alkoxide that is responsible for the positioning of the site of oxidative attack towards the N5 of the flavin and thereby enables hydride transfer. The residue pairs Gln438/Asn411 and Arg292/Asn411 complex two water molecules that additionally may contribute to this hydrophilic pocket. Additionally, the individual contribution to $\Delta\Delta G_T^\ddagger$ (see Table 3) of each residue can be taken into account to explain their role. For the variants Gln438Val and Arg292Met an increase in $\Delta\Delta G_T^\ddagger$ 11 and 9 kJ/mol was calculated. According to our MD-simulations these residues interact directly with the alkoxy intermediate and therefore the variation of these residues exhibits the most pronounced effects on catalysis. Other residues like Asn411, Tyr117 and Lys436 contribute rather to the establishment of the network and to the fine tuning and positioning of the key residues Tyr193, Tyr479, Arg292 and Gln438. Likewise, also the pKa of the allylic alcohol of the substrate is anticipated to be influenced by the same set of residues.

3.10. Conservation of the active site residues in plant kingdom

Previously, we have defined four different active site types occurring within the family of BBE-like proteins in plants. Most abundant are type I and IV; the type IV is found in monocotyledons, while type I, as present in AtBBE15, is predominant in dicotyledons [6]. While the residues corresponding to Gln438 and Arg292, which directly interact with the alkoxide intermediate, are conserved in these active site types, the mechanism of proton abstraction varies [6,35]. Well characterized enzymes bearing a type IV active site are Phl p 4, GOOX or PpBBE1 [21,22,36]. To compare both active site types an overlay of AtBBE15 and Phl p 4

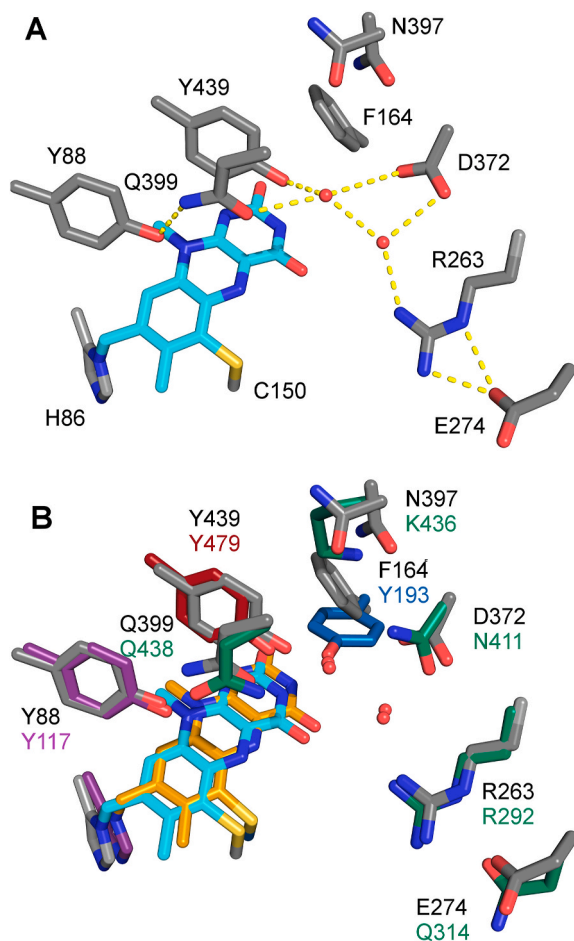


Fig. 8. Comparison of BBE-like protein active site type I and IV. A: Hydrogen bond network in type I (Phl p 4, pdb code 3tsh), B: overlay of AtBBE15 and Phl p 4.

was created, also the respective hydrogen bond network in the active site of Phl p 4 is visualized in Fig. 8.

Like in AtBBE15 an excessive hydrogen bond network connecting Tyr88 with Glu274 is present in the active site of Phl p 4 including two water molecules. Tyr88 interacts with Gln399, which is in hydrogen bond distance to a water molecule interacting with Tyr439 and Asp372. Another water molecule is complexed between Asp372 and Arg263, which is in hydrogen bond distance to Glu274. The topology of this network strongly resembles that of AtBBE15 where the residues interacting with a putative alkoxide intermediate are found to be spatially and sequentially conserved. Therefore, the formation of an alkoxide binding site is not restricted to the type I active site but is to be anticipated as a general feature of BBE-like proteins from plants. The proton abstraction was postulated differently in the active site type IV [36] with Tyr439 acting as a catalytic base that is activated by Asp372 by deprotonation via a water molecule. Apparently, BBE-like proteins with an active site of type I or IV predominantly catalyze the oxidation of alcohols suggesting a common mode of intermediate stabilization, however the mechanism of substrate deprotonation may differ. To evaluate how conserved the respective residues are in mono- and di-cotyledons, sequences of BBE-like proteins were retrieved from Phytozome and a sequence alignment was generated using Clustal omega and edited by hand using Jalview. The two most abundant residues were extracted for the different active site forming positions and are summarized in Table 6.

In monocotyledons the active site composition described for Phl p 4 is well conserved with a degree of conservation for the different position

Table 6

Active site composition of BBE-like proteins from mono- and dicotyledons.

Residue from AtBBE15	Monocotyledons	Dicotyledons
	Consensus [residue: %]	
Tyr193	Phe: 71, Ile: 23	Tyr: 79, Phe: 11
Tyr479	Tyr 92, Phe: 7	Tyr: 94, Phe: 4
Lys436	Asn: 71, Gln: 10	Lys: 53, Met: 15
Tyr117	Tyr: 93, Leu: 2	Tyr 74, Phe: 20
Gln438	Gln: 98, Glu: 1	Gln 64, Leu: 9
Asn411	Asp: 70, Glu: 25	Asn 51, Thr: 19
Arg292	Arg: 77, Ser: 16	Arg 80, His: 5
Gln314	Asp: 79, Asn: 17	Asn 28, Ile: 15

varying from 70% to 98% implying that a reaction mechanism postulated for Phl p 4 can putatively also be applied to the majority of all BBE-like proteins from monocotyledons. In dicotyledons the active site composition is more diverse, more than one active site type has been described so far and more can be extracted from the alignment that are not to be covered in this report. Typically, the positions corresponding to Tyr193, Tyr479 and Tyr117 are occupied by a Tyr/Phe with conservation of 79/11, 94/4 and 74/20%, respectively. Arg292 and Gln438, that are postulated to interact directly with the alkoxide intermediate are found in 80% and 64% of the sequences, respectively. Therefore, there is a higher degree of plasticity in the active site composition of BBE-like proteins from dicotyledons, nevertheless the key residues Tyr193, Tyr479, Arg292 and Gln438 are well conserved and a similar mechanism as proposed for AtBBE15 can be anticipated for the majority of BBE-like proteins from plants.

4. Conclusion

Previously, we have postulated an enzymatic mechanism of monolignol oxidoreductases based on their structure and activity. In this report, we have refined this mechanism based on kinetic data generated by a comprehensive site directed mutagenesis program. We postulate a stepwise mechanism in which the substrate is activated via proton abstraction and the corresponding alkoxide intermediate is oxidized by hydride transfer. We have identified an excessive hydrogen bond network in the active site of AtBBE15 containing Tyr193 and Tyr479 acting concertedly as catalytic base. Based on the pH-dependency of the activity of the variants, we have outlined the importance of Lys436, Arg292 and Gln438 for the fine tuning of the pK_a of Tyr193 and Tyr479. We have also conducted MD-simulations to evaluate binding modes of coniferyl alcohol and the corresponding alkoxide. The simulations have revealed that two different distinct binding modes exist, while the alcohol predominantly interacts with Tyr193 and Tyr479, the alkoxide in complexed by Gln438, Arg292 and Tyr193. By means of sequence alignments, we have demonstrated that this alkoxide binding site is a highly conserved universal feature of BBE-like proteins from plants and, therefore, the mechanism we have postulated is relevant not only for AtBBE15 but for the majority of the BBE-like proteins. Our work has substantially broadened the understanding of BBE-like proteins and demonstrated that AtBBE15 represents a suitable paradigm for this whole class of proteins.

Appendix A. Supplementary data

Supplementary data to this article can be found online at <https://doi.org/10.1016/j.abb.2021.108766>.

This work was supported by a grant from the Austrian Science Foundation (FWF) (Doctoral program ‘‘Molecular Enzymology’’ W908 and P28678) to KG and PM. We would like to acknowledge the help of Marina Toplak by her expertise in methodology and scientific input.

Author contributions

Julia Messenlehner: Collected the data, performed stopped-flow experiments, steady state kinetics, recorded spectra, performed the analysis, wrote the paper. Michael Hetmann: Collected the data performed MD-Simulations, performed docking experiments, performed the analysis, wrote the paper. Adrian Tripp: Collected the data of steady-state kinetics, performed the analysis. Silvia Wallner: Collected the data, cloning, screened expression strains, performed the analysis. Peter Macheroux: Conceived and designed the analysis, wrote the paper. Karl Gruber: Contributed data or analysis tools, calculated the pH-optima, performed the analysis, wrote the paper. Bastian Daniel: Collected the data, cloning, mutagenesis, screening of expression strains, enzyme production, stopped flow kinetics, performed the analysis, wrote the paper.

References

- R.L. Fagan, B.A. Palfey, Flavin-Dependent Enzymes. Comprehensive Natural Products II, Elsevier, 2010, pp. 37–113, <https://doi.org/10.1016/B978-008045382-8.00135-0>.
- P. Macheroux, B. Kappes, S.E. Ealick, Flavogenomics - a genomic and structural view of flavin-dependent proteins, *FEBS J.* 278 (2011) 2625–2634, <https://doi.org/10.1111/j.1742-4658.2011.08202.x>.
- M.W. Fraaije, A. Mattevi, Flavoenzymes: diverse catalysts with recurrent features, *Trends Biochem. Sci.* 25 (2000) 126–132, [https://doi.org/10.1016/S0968-0004\(99\)01533-9](https://doi.org/10.1016/S0968-0004(99)01533-9).
- E. Romero, G. Gadda, Alcohol oxidation by flavoenzymes, *Biomol. Concepts* 5 (2014) 299–318, <https://doi.org/10.1515/bmc-2014-0016>.
- B. Daniel, T. Pavkov-Keller, B. Steiner, A. Dordic, A. Gutmann, B. Nidetzky, et al., Oxidation of monolignols by members of the berberine bridge enzyme family suggests a role in plant cell wall metabolism, *J. Biol. Chem.* 290 (2015) 18770–18781, <https://doi.org/10.1074/jbc.M115.659631>.
- B. Daniel, B. Konrad, M. Toplak, M. Lahham, J. Messenlehner, A. Winkler, et al., The family of berberine bridge enzyme-like enzymes: a treasure-trove of oxidative reactions, *Arch. Biochem. Biophys.* 632 (2017) 88–103, <https://doi.org/10.1016/j.abb.2017.06.023>.
- A. Winkler, A. Lyskowski, S. Riedl, M. Puhl, T.M. Kutchan, P. Macheroux, et al., A concerted mechanism for berberine bridge enzyme, *Nat. Chem. Biol.* 4 (2008) 739–741, <https://doi.org/10.1038/nchembio.123>.
- P. Steffens, N. Nagakura, M.H. Zenk, The berberine bridge forming enzyme in tetrahydroprotoberberine biosynthesis, *Tetrahedron Lett.* 25 (1984) 951–952, [https://doi.org/10.1016/S0040-4039\(01\)80070-8](https://doi.org/10.1016/S0040-4039(01)80070-8).
- R. Hille, S. Miller, B. Palfey (Eds.), *Handbook of Flavoproteins*. Berlin, Boston, DE GRUYTER, 2012, <https://doi.org/10.1515/9783110268911>.
- G. Steinkellner, R. Rader, G.G. Thallinger, C. Kratky, K. Gruber, VASCO: computation and visualization of annotated protein surface contacts, *BMC Bioinform.* 10 (2009) 32, <https://doi.org/10.1186/1471-2105-10-32>.
- M. Hendlich, F. Rippmann, G. Barnickel, LIGSITE: automatic and efficient detection of potential small molecule-binding sites in proteins, *J. Mol. Graph. Model.* 15 (1997) 359–363, [https://doi.org/10.1016/S1093-3263\(98\)00002-3](https://doi.org/10.1016/S1093-3263(98)00002-3).
- S. Gandomkar, E. Jost, D. Loidolt, A. Swoboda, M. Pickl, W. Elailly, et al., Biocatalytic enantioselective oxidation of sec-allylic alcohols with flavin-dependent oxidases, *Adv. Synth. Catal.* 361 (2019) 5264–5271, <https://doi.org/10.1002/adsc.201900921>.
- R. Weis, R. Lutten, W. Skranc, H. Schwab, M. Wubbolts, A. Glieder, Reliable high-throughput screening with by limiting yeast cell death phenomena, *FEMS Yeast Res.* 5 (2004) 179–189, <https://doi.org/10.1016/j.femsyr.2004.06.016>.
- G.M. Morris, D.S. Goodsell, R.S. Halliday, R. Huey, W.E. Hart, R.K. Belew, et al., Automated docking using a Lamarckian genetic algorithm and an empirical binding free energy function, *J. Comput. Chem.* 19 (1998) 1639–1662, [https://doi.org/10.1002/\(SICI\)1096-987X\(19981115\)19:14<1639::AID-JCC10>3.0.CO;2-B](https://doi.org/10.1002/(SICI)1096-987X(19981115)19:14<1639::AID-JCC10>3.0.CO;2-B).
- M. Bergdorf, S. Baxter, C.A. Rendleman, D.E. Shaw, Desmond/GPU Performance as of November 2016, *D E Shaw Res Tech Rep DESRES/TR-2015-01*, 2015.
- D.M. Goodstein, S. Shu, R. Howson, R. Neupane, R.D. Hayes, J. Fazo, et al., Phytozome: a comparative platform for green plant genomics, *Nucleic Acids Res.* 40 (2012) D1178–D1186, <https://doi.org/10.1093/nar/gkr944>.
- F. Sievers, A. Wilm, D. Dineen, T.J. Gibson, K. Karplus, W. Li, et al., Fast, scalable generation of high-quality protein multiple sequence alignments using Clustal Omega, *Mol. Syst. Biol.* 7 (2011) 539, <https://doi.org/10.1038/msb.2011.75>.
- A.M. Waterhouse, J.B. Procter, D.M.A. Martin, M. Clamp, G.J. Barton, Jalview Version 2—a multiple sequence alignment editor and analysis workbench, *Bioinformatics* 25 (2009) 1189–1191, <https://doi.org/10.1093/bioinformatics/btp033>.
- P.F. Heelis, The photophysical and photochemical properties of flavins (isoalloxazines), *Chem. Soc. Rev.* 11 (1982) 15, <https://doi.org/10.1039/cs9821100015>.
- G. Gygli, W.J.H. Berkel van, Communication. Vanillyl alcohol oxidases produced in Komagataella phaffii contain a highly stable noncovalently bound anionic FAD semiquinone, *Biocatalysis* 3 (2017), <https://doi.org/10.1515/boca-2017-0002>.
- M. Toplak, G. Wiedemann, J. Uličević, B. Daniel, S.N.W. Hoernstein, J. Kothe, et al., The single berberine bridge enzyme homolog of Physcomitrella patens is a cellobiose oxidase, *FEBS J.* 285 (2018) 1923–1943, <https://doi.org/10.1111/febs.14458>.
- D. Zafred, A. Nandy, L. Pump, H. Kahlert, W. Keller, Crystal structure and immunologic characterization of the major grass pollen allergen Phl p 4, *J. Allergy Clin. Immunol.* 132 (2013) 696–703, <https://doi.org/10.1016/j.jaci.2013.03.021>, e10.
- A. Winkler, F. Hartner, T.M. Kutchan, A. Glieder, P. Macheroux, Biochemical evidence that berberine bridge enzyme belongs to a novel family of flavoproteins containing a Bi-covalently attached FAD cofactor, *J. Biol. Chem.* 281 (2006) 21276–21285, <https://doi.org/10.1074/jbc.M603267200>.
- T.A. Ewing, Q.-T. Nguyen, R.C. Allan, G. Gygli, E. Romero, C. Binda, et al., Two tyrosine residues, Tyr-108 and Tyr-503, are responsible for the deprotonation of phenolic substrates in vanillyl-alcohol oxidase, *J. Biol. Chem.* 292 (2017) 14668–14679, <https://doi.org/10.1074/jbc.M117.778449>.
- A.R. Fersht, R.J. Leatherbarrow, T.N.C. Wells, Quantitative analysis of structure–activity relationships in engineered proteins by linear free-energy relationships, *Nature* 322 (1986) 284–286, <https://doi.org/10.1038/322284a0>.
- A.R. Fersht, R.J. Leatherbarrow, T.N.C. Wells, Structure-activity relationships in engineered proteins: analysis of use of binding energy by linear free energy relationships, *Biochemistry* 26 (1987) 6030–6038, <https://doi.org/10.1021/bi00393a013>.
- S. Pils, K. Schnabl, S. Wallner, M. Kljajic, N. Kupresanin, R. Breinbauer, et al., Characterization of the monolignol oxidoreductase AtBBE-like protein 15 L182V for biocatalytic applications, *J. Mol. Catal. B Enzym.* 133 (2016) S6–S14, <https://doi.org/10.1016/j.molcatb.2016.10.018>.
- W.W. Cleland, The low-barrier hydrogen bond in enzymic catalysis, *Adv. Phys. Org. Chem.* (2010) 1–17, [https://doi.org/10.1016/S0065-3160\(08\)44001-7](https://doi.org/10.1016/S0065-3160(08)44001-7).
- R. Miura, Versatility and specificity in flavoenzymes: control mechanisms of flavin reactivity, *Chem. Rec.* 1 (2001) 183–194, <https://doi.org/10.1002/tcr.1007>.
- A. Martinière, R. Gibrat, H. Sentenac, X. Dumont, I. Gaillard, N. Paris, Uncovering pH at both sides of the root plasma membrane interface using noninvasive imaging, *Proc. Natl. Acad. Sci.* 115 (2018) 6488–6493, <https://doi.org/10.1073/pnas.1721769115>.
- M.J. Minch, An introduction to hydrogen bonding (Jeffrey, George A.), *J. Chem. Educ.* 76 (1999) 759, <https://doi.org/10.1021/ed076p759.1>.
- E.N. Baker, R.E. Hubbard, Hydrogen bonding in globular proteins, *Prog. Biophys. Mol. Biol.* 44 (1984) 97–179, [https://doi.org/10.1016/0079-6107\(84\)90007-5](https://doi.org/10.1016/0079-6107(84)90007-5).
- P.F. Fitzpatrick, Combining solvent isotope effects with substrate isotope effects in mechanistic studies of alcohol and amine oxidation by enzymes, *Biochim. Biophys. Acta Protein Proteomics* 1854 (2015) 1746–1755, <https://doi.org/10.1016/j.bbapap.2014.10.020>.
- G. Gadda, Hydride transfer made easy in the reaction of alcohol oxidation catalyzed by flavin-dependent oxidases, *Biochemistry* (2008), <https://doi.org/10.1021/bi801994c>.
- B. Daniel, S. Wallner, B. Steiner, G. Oberdorfer, P. Kumar, E. van der Graaff, et al., Structure of a berberine bridge enzyme-like enzyme with an active site specific to the plant family brassicaceae. van Berkel WJH, *PLoS One* 11 (2016), e0156892, <https://doi.org/10.1371/journal.pone.0156892>.
- C.-H. Huang, W.-L. Lai, M.-H. Lee, C.-J. Chen, A. Vasella, Y.-C. Tsai, et al., Crystal structure of glucooligosaccharide oxidase from *Acremonium strictum*, *J. Biol. Chem.* 280 (2005) 38831–38838, <https://doi.org/10.1074/jbc.M506078200>.